Theoretical Analysis of AM and FM Interference Robustness of Integrating DDR Receiver for Human Body Communication

Shovan Maity, *Student Member, IEEE*, Xinyi Jiang, *Student Member, IEEE*, and Shreyas Sen, *Senior Member, IEEE*

***Abstract*—Prolific growth of miniaturized devices has led to widespread use of wearable devices and physiological sensors. The state-of-art technique for connecting these devices and sensors is through wireless radio waves. However, wireless body area wireless body area network (WBAN) suffers from limited security (wireless signals from energy-constrained sensors can be snooped by nearby attackers), poor energy-efficiency (up conversion and down conversion), and self-interference. Human body communication (HBC), which uses human body as a conducting medium, has emerged as a new alternative physical layer for WBAN, as it can enable communication with better energy efficiency and enhanced security. Broadband (BB) HBC uses the human body channel as a broadband communication medium and can enable higher energy efficiency compared to narrowband HBC. However, due to the antenna effect of human body, ambient interferences get picked up from the environment, proving to be one of the primary bottlenecks for BB-HBC systems. In this paper, we analyze the performance of an integrating dual data rate (I-DDR) receiver, which enables interference robust BB-HBC, under continuous wave (CW), amplitude modulated (AM), and frequency modulated (FM) interferences. Theoretical derivations along with simulations provide key insights into the behavior of I-DDR receiver under different interference scenarios, highlighting the efficacy (>22 dB improvement in SIR tolerance for both FM and AM) of the technique. Finally, measurements are carried out by applying the I-DDR principle on signals transmitted through the human body and captured on an oscilloscope. Measurements from an I-DDR receiver fabricated in TSMC 65 nm technology shows $<10^{-4}$ BER in presence of CW, AM, and FM interference with −21 dB SIR further demonstrating the efficacy of the I-DDR method in interference rejection.**

***Index Terms*—Energy-efficiency, human body communication, interference rejection, security.**

Manuscript received December 17, 2018; revised January 26, 2019; accepted March 5, 2019. Date of publication April 15, 2019; date of current version May 24, 2019. This work was supported in part by the Air Force Office of Scientific Research YIP Award under Grant FA9550-17-1-0450 and in part by the National Science Foundation CRII Award under Grant CNS 1657455. The paper was recommended by Associate Editor H. Jiang. *(Corresponding author: Shovan Maity.)*

S. Maity and S. Sen are with the School of Electrical and Computer Engineering, Purdue University, West Lafayette, IN 47907 USA (e-mail: maity@purdue.edu; shreyas@purdue.edu).

X. Jiang is with the Department of Electrical Engineering and Computer Sciences, University of California, Berkeley, CA 94720-5800 USA (e-mail: jiang330@purdue.edu).

Color versions of one or more of the figures in this paper are available online at http://ieeexplore.ieee.org.

Digital Object Identifier 10.1109/TBCAS.2019.2911475

I. Introduction

With the advancement of semiconductor technology, the size of wearable devices has reduced drastically, accelerating the usage of wearable sensors and smart devices (e.g., Smart watches, Fitness trackers). Wireless Body Area Network (WBAN) is the state-of-art technology for connectivity between these sensors and computing devices. However, WBAN communication based on radio waves, suffers from limited security, low energy-efficiency and self-interference. Recently, Human Body Communication (HBC) has emerged as an alternate physical layer for communication to connect these devices. HBC, which utilizes the human body as a medium for interconnecting wearable devices, offers increased security along with ultra-low power (ULP) demand. Human body as a conducting medium exhibits lower loss compared to radio frequency propagation through air, enabling HBC's ULP property. Also in HBC, most of the signal transmission is confined within the human body as the signal is not broadcasted in the wireless medium as in WBAN. This enables higher security in HBC as it is harder for an attacker to snoop the ongoing transmission. These advantages enable HBC to be used for applications such as physiological sensing, secure authentication and social networking [1].

However due to the antenna properties of the human body, it picks up ambient signals from the environment as interference, which turns out to be one of the primary bottlenecks for HBC. Several signaling techniques have been proposed as a solution, such as Adaptive Frequency Hopping (AFH) [2] and fixed narrowband signaling [3]. But all of these techniques suppress the undesired interference by avoiding the interference frequency band using narrowband signaling, which requires bulky filters and relatively higher power. Recently, an alternative way to circumvent the interference, using resettable integration with dual data rate (DDR) NRZ receiver, has been proposed in [1]. In this paper, we analyze the performance of the Integrating DDR (I-DDR) receiver in the presence of Continuous Wave (CW), Amplitude Modulated (AM) and Frequency Modulated (FM) interference and show its interference rejection property. The key contribution of the paper is the important insights into the behavior of I-DDR receiver under different interference scenarios, highlighting its efficacy (>22 dB improvement in integrated SIR for both FM and AM interferences) supported by theoretical derivation, simulations and hardware experiments using

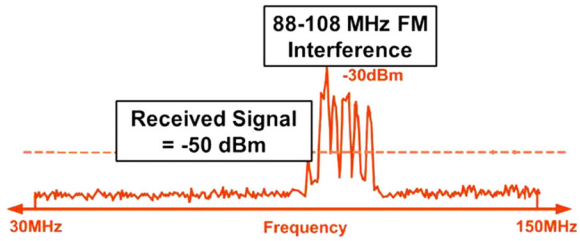

Fig. 1. Frequency spectrum of FM signal acting as an interference source for HBC.

Commercial-Off-The-Shelf (COTS) components and Integrated Circuits.

The rest of the paper is organized as follows. Section II provides the background and motivation for using I-DDR receiver for HBC. The theoretical derivations and simulation results of the I-DDR receiver for different interference is presented in Section III, Section IV and Section V discusses measurement setup and measurement results evaluating the interference rejection property with conclusion in Section VI.

II. Interference-Robust ULP HBC

A. HBC Channel Models

The human body channel characteristics is one of the key aspects of HBC. There have been several studies focusing on measuring the human body channel loss with varying frequency. These studies show a wide variation in the measured channel response due to the prominent effect of measurement setup on the results. Some of the studies [4]–[8] characterize the body as a high pass channel due to the low impedance termination (50Ω termination from Spectrum Analyzer, Vector Network Analyzer) provided at the receiver end. There are also a few studies which characterize the human body as a low loss channel due to improper ground isolation between the transmitter and receiver [4], [9]. Recently, it is shown that a capacitive high impedance termination at the receiver end enables the human body to be used as a broadband channel [10]–[12]. This has enabled the design of a Broadband I-DDR receiver, which enhances the energy efficiency of HBC by utilizing the complete bandwidth of the body for data transmission and eliminating the need of frequency up and down conversion. In this paper, we focus on analyzing the robustness of the I-DDR HBC receiver with NRZ signaling under continuous wave, AM and FM interferences.

B. Interference on Human Body

The human body picks up ambient signals as interference due to its antenna property. Previous studies have shown that the antenna properties are present in the 40–400 MHz frequency range (Figure 1) [2]. The FM radio frequency band (88–108 MHz) falls within this range, making it one of the primary sources of interference. Several narrowband signaling techniques [2], [3], [13], [14] have been proposed to suppress this interference, such as Adaptive frequency hopping (AFH) [2] and fixed multi-carrier narrowband signaling [6] etc. But these techniques require frequency up-conversion for modulation and down conversion for demodulation, which increases circuit power consumption. Also unlike a broadband transmission, these narrowband techniques utilizes a fraction of the available bandwidth, which makes them inherently less energy efficient. Since the human body can possibly be used as a broadband channel, broadband HBC techniques has been proposed which uses NRZ signaling [1] or multi-level Walsh Coding [15] to send broadband data through the body. This enables a higher rate of data transfer while operating at lower frequencies and hence can improve the energy efficiency of transmission. However, interference will affect broadband transmission more than a narrowband transmission. In [15] a band stop filter has been used to reject interference from the FM band, but it would require multiple band stop filters to block any other interference on a different frequency band. An Integrating Dual Data Rate (I-DDR) receiver [1], on the other hand enables interference robust broadband operation without requiring any extra filters. In the following sections we analyze and evaluate the interference rejection property of the I-DDR receiver in presence of different kind of interferences through simulations and theoretical derivations.

III. Interference-Robustness of Integrating DDR Rx

In this section, we discuss the working principle of the integrating DDR (I-DDR) receiver and analyze it's interference-rejection property with NRZ signaling in presence of CW, AM and FM interferences.

Analysis of I-DDR principle: CW interference

$$S_{RX} = S_{sig} + S_{intf} \tag{1}$$

$$S_{sig}(t) = \pm A_{sig} \qquad 0 \le t \le T_b \tag{2}$$

$$S_{intf}(t) = A_{intf} \sin(\omega_i t + \varphi) \qquad \forall\, t$$

$$\omega_i = \frac{2\pi}{T_i} = \text{Interference frequency}$$

$$\varphi = \text{Phase difference between signal and interference} \tag{3}$$

$$IS_{sig}(t) = \int_0^t S_{sig} = \begin{cases} \pm K_{int} A_{sig} t, & 0 \le t \le T_b \\ 0, & T_b \le t \le 2T_b \end{cases}$$

$$K_{int} = \text{Integrator Gain} \tag{4}$$

$$IS_{intf}(t) = \int_0^t S_{intf} = \begin{cases} -K_{int} \frac{A_{intf} cos(\omega_i t + \varphi)}{\omega_i}, & 0 \le t \le T_b \\ 0, & T_b \le t \le 2T_b \end{cases} \tag{5}$$

$$IS_{sig}|_{t=T_b} = \pm K_{int} A_{sig} T_b \tag{6}$$

$$IS_{intf}|_{t=T_b} = K_{int} \frac{A_{intf}\left[\cos(\varphi) - cos(\omega_i T_b + \varphi)\right]}{\omega_i} = 0, \forall T_b = nT_i;\ n = \text{positive integer} \tag{7}$$

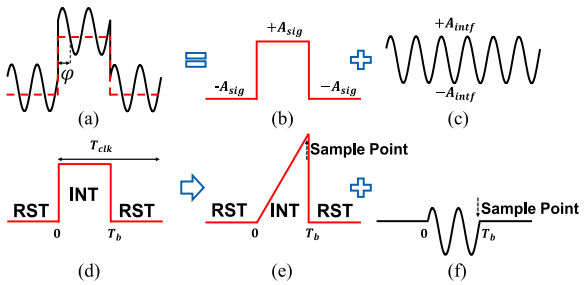

Fig. 2. Working principle of Integrating DDR receiver as a notch filter for interference suppression a) NRZ signal + CW interference can be decomposed as a superposition of b) and c) d) Integration clock: each integration period is followed by a reset period, leading to the need for two parallel receiver paths, i.e., dual-data rate (DDR) receiver. $T_{clk} = 2T_b$ e) Integrated NRZ signal f) Integrated interference is 0 for $T_b = nT_i$ (shown for $T_b = 2T_i$).

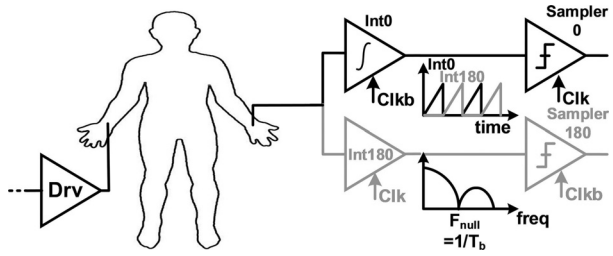

Fig. 3. Transceiver diagram for Interference robust HBC. A dual data rate (DDR) receiver with a resettable integrator followed by a sampler is used.

A. Working Principle

Figure 2 illustrates the working principle of I-DDR receiver with an NRZ signal in presence of a CW interference [1]. Commonly, in HBC, the interference strength (A_{intf}) is significantly greater than the signal amplitude (A_{sig}). The large difference often leads to a closed eye-diagram of the received signal, making it hard to sample accurately, increasing Bit Error Rate (BER). However, the I-DDR receiver can be used to process the signal to achieve an open eye, which will enable accurate sampling and significantly reduce BER. The I-DDR receiver integrates the received signal over a fixed period and samples it at the end of the period. The integration period is chosen as a multiple of the interference period, such that the interference signal is canceled during sampling and the sampled value is determined only by the NRZ signal. Since, the integration operation accumulates the signal information over time, it is necessary to reset the integrator at the end of an integration operation and before the beginning of the next. This ensures the decoded value at the end of the current period is not affected by any previous data bits. To achieve this operation, the receiver has two phases: 1) Integration phase and 2) Reset phase. The circuit implementation of the transceiver is shown in Figure 3. Since each integrator integrates for one phase of the clock and is reset for the alternate phase $(T_{clk} = 2T_b)$, two phases of clock are required to integrate consecutive symbols, resulting in a dual data rate (DDR) receiver. The integrator is reset every bit period and the integrated signal is sampled just before the reset. The receiver consists of two chains, each consisting of an integrator followed by a sampler. The operating clock for each of these chains is 180 degree out of phase. So, when one of the integrators is in Reset phase the other one is in the Integration phase. By doing integration and choosing the bit period (T_b) appropriately as an integral multiple of the interference signal period (T_i), $T_b = nT_i$, the interference can be nullified. The detailed analysis of the interference rejection principle of I-DDR receiver is discussed in the following subsections.

B. Continuous Wave (CW) Interference

This section looks into the mathematical analysis of I-DDR receiver in presence of CW interference. The received signal (S_{RX}) (1) is a linear superposition of the desired NRZ signal (S_{sig}) (2) and the undesired interference (S_{intf}) (3). The signal is integrated before being applied to a sampler for decoding. The integrated signal is also a linear superposition of the integrated signal (4) and integrated interference (5). Since the integrating receiver samples the signal at the end of the bit period (T_b), the sampled integrated data and interference at $t = T_b$ is provided in (6) and (7). If the data rate is chosen such that the bit period is an integral multiple of the interference period $(T_b = nT_i)$, the integrated interference equals 0 for any arbitrary phase of the input signal (φ), as shown in (7). In an ideal scenario, the interference can be suppressed completely by choosing the bit period equal to integral multiple of the interference period through integration. This is the fundamental basis of using Integrating DDR (I-DDR) receiver for interference suppression in HBC. Figure 4a shows a plot of the integrated interference (IS_{intf}) for different integration period, represented as a fraction of the interference time period. It can be seen that, if the data rate is chosen to be an integral multiple of interference $(T_b = nT_i)$ the integrated interference is 0 irrespective of the initial phase of the signal. Figure 4b shows the relative interference rejection, which is defined as the ratio of integrated interference to integrated signal at the sampling instant, as a function of varying interference frequency for a fixed data frequency of 100 MHz. There are nulls for all frequencies which correspond to an integral multiple of the data frequency irrespective of the initial phase of the signal. Also, it can be seen that the I-DDR receiver can provide >15dB rejection even for interference frequency mismatch of 10% (90 MHz, 110 MHz for data frequency of 100 MHz). In an actual implementation, the interference frequency will not always be an integral multiple of the applied data signal. However, the interference rejection of the I-DDR receiver for CW signals shows it's applicability for such scenarios also.

Key Takeaway: Figure 4b shows that there are notches in the transfer function of the I-DDR receiver in presence of continuous wave interference which are dependent on the initial phase of the signal. However the transfer function notches corresponding to data frequency $(f = \frac{1}{T_b})$ and its integral multiples are present irrespective of the initial phase of the interference and hence it can be used to reject interference at that frequency.

C. Amplitude Modulated (AM) Interference

This section looks into the analysis of I-DDR receiver performance in presence of AM interference. The interference signal (S_{intf}) and the integrated interference (IS_{intf}) are presented as in (8), (9) respectively. The sampled interference at the end of the data period is provided in (10).

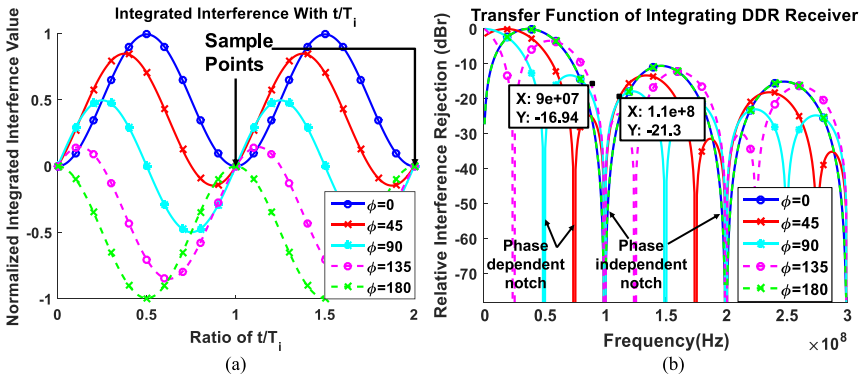

Fig. 4. Perofrmance analysis of I-DDR receiver under CW interference ($f_i = 100$ MHz) a) Normalized integrated interference (IS_{intf}) as a function of $\frac{t}{T_i}$ ($f_i = 100$ MHz) b) Interference suppression as a function of interference frequency with data frequency of 100 MHz.

Analysis of I-DDR principle: AM interference

$$S_{intf}(t) = A_{intf}\sin(\omega_i t+\varphi) + \frac{A_{intf}M}{2}\left[\sin\left(\left(\omega_i+\omega_m\right)t+\varphi+\varphi_m\right)+\sin\left(\left(\omega_i-\omega_m\right)t+\varphi-\varphi_m\right)\right] \quad \forall t$$
$$\omega_i = \frac{2\pi}{T_i} = \text{Carrier Wave Frequency},\ \omega_m = \frac{2\pi}{T_m} = \text{Modulation Wave Frequency},\quad M = \text{Modulation Index} \tag{8}$$

$$IS_{intf} = \begin{cases} -\frac{K_{int}A_{intf}}{\omega_i}\cos(\omega_i t+\varphi) - \frac{K_{int}A_{intf}M}{2(\omega_i+\omega_m)}\cos\left(\left(\omega_i+\omega_m\right)t+\varphi+\varphi_m\right) \\ -\frac{K_{int}A_{intf}M}{2(\omega_i-\omega_m)}\cos\left(\left(\omega_i-\omega_m\right)t+\varphi-\varphi_m\right), & 0\le t\le T_b \\ 0, & T_b\le t\le 2T_b \end{cases} \tag{9}$$

$$\begin{aligned} IS_{intf}|_{t=T_b} &= \frac{K_{int}A_{intf}}{\omega_i}\left[\cos(\varphi)-\cos(\omega_i T_b+\varphi)\right] + \frac{K_{int}A_{intf}M}{2(\omega_i+\omega_m)}\left[\cos(\varphi+\varphi_m)-\cos\left(\left(\omega_i+\omega_m\right)T_b+\varphi+\varphi_m\right)\right] \\ &\quad + \frac{K_{int}A_{intf}M}{2(\omega_i-\omega_m)}\left[\cos(\varphi-\varphi_m)-\cos\left(\left(\omega_i-\omega_m\right)T_b+\varphi-\varphi_m\right)\right] \\ &= \text{residual}_a + \text{residual}_b, \forall\ T_b = nT_i;\ n = \text{positive integer} \end{aligned} \tag{10}$$

$$\text{residual}_a = \frac{K_{int}A_{intf}M}{2(\omega_i+\omega_m)}\left[\cos(\varphi+\varphi_m)-\cos\left(2\pi\frac{T_b}{T_m}+\varphi+\varphi_m\right)\right]$$
$$\text{residual}_b = \frac{K_{int}A_{intf}M}{2(\omega_i-\omega_m)}\left[\cos(\varphi-\varphi_m)-\cos\left(-2\pi\frac{T_b}{T_m}+\varphi-\varphi_m\right)\right]$$

$$\begin{aligned} \text{For } \varphi=\tfrac{\pi}{2}:\ IS_{intf}|_{t=T_b} &= \frac{K_{int}A_{intf}M}{2(\omega_i+\omega_m)}\left[-\sin(\varphi_m)+\sin\left(2\pi\frac{T_b}{T_m}+\varphi_m\right)\right] + \frac{K_{int}A_{intf}M}{2(\omega_i-\omega_m)}\left[\sin(\varphi_m)-\sin\left(2\pi\frac{T_b}{T_m}+\varphi_m\right)\right] \\ &= K_{int}A_{intf}M\frac{\omega_m}{\omega_i^2-\omega_m^2}\left[\sin(\varphi_m)\left(1-\cos\left(2\pi\frac{T_b}{T_m}\right)\right)-\cos(\varphi_m)\sin\left(2\pi\frac{T_b}{T_m}\right)\right] \end{aligned} \tag{11}$$

$$\begin{aligned} \text{For } \varphi_m=\pi:\ IS_{intf}|_{t=T_b} &= \frac{K_{int}A_{intf}M}{2(\omega_i+\omega_m)}\left[-\cos(\varphi)+\cos\left(2\pi\frac{T_b}{T_m}+\varphi\right)\right] + \frac{K_{int}A_{intf}M}{2(\omega_i-\omega_m)}\left[-\cos(\varphi)+\cos\left(-2\pi\frac{T_b}{T_m}+\varphi\right)\right] \\ &= K_{int}A_{intf}M\frac{\omega_m}{\omega_i^2-\omega_m^2}sin(\varphi)\sin\left(2\pi\frac{T_b}{T_m}\right) + K_{int}A_{intf}M\frac{\omega_i}{\omega_i^2-\omega_m^2}\cos(\varphi)\left[\cos\left(2\pi\frac{T_b}{T_m}\right)-1\right] \end{aligned} \tag{12}$$

$$\text{SIR without integration} = \frac{\pm A_{sig}}{A_{intf}\sin(\omega_i T_b+\varphi) + \frac{A_{intf}M}{2}\left[\sin\left(\left(\left(\omega_i+\omega_m\right)T_b+\varphi+\varphi_m\right)+\sin\left(\left(\omega_i-\omega_m\right)T_b+\varphi-\varphi_m\right)\right)\right]} \tag{13}$$

$$\text{Integrated SIR} = \frac{\pm A_{sig}T_b}{\frac{A_{intf}M}{2(\omega_i+\omega_m)}\left[\cos(\varphi+\varphi_m)-\cos\left(2\pi\frac{T_b}{T_m}+\varphi+\varphi_m\right)\right] + \frac{A_{intf}M}{2(\omega_i-\omega_m)}\left[\cos(\varphi-\varphi_m)-\cos\left(-2\pi\frac{T_b}{T_m}+\varphi-\varphi_m\right)\right]} \tag{14}$$

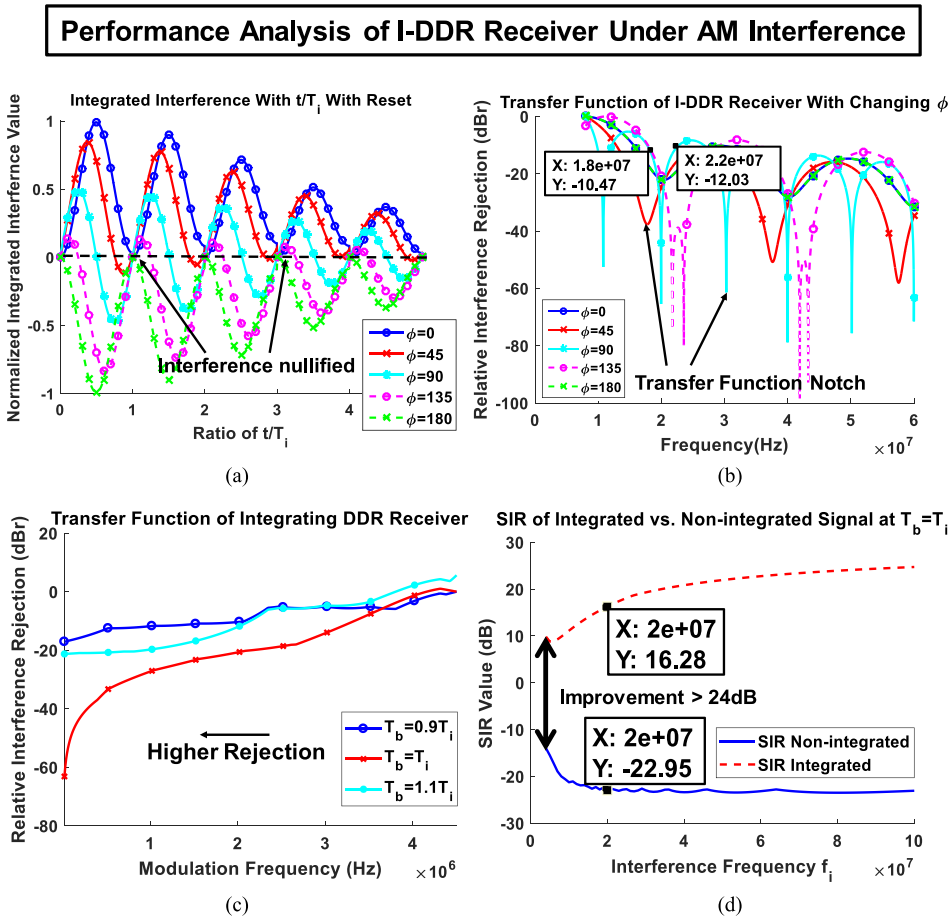

Fig. 5. Performance analysis of I-DDR receiver under AM interference ($M = 0.5, f_i, f_b = 20$ MHz, $f_m = 2$ MHz). a) Integrated interference (IS_{intf}) as a function of $\frac{t}{T_i}$ b) Interference suppression as a function of interferer frequency with changing φ c) Worst case of Interference rejection as a function of f_m with $\pm 10\%$ variation in sampling instant d) SIR of Integrated vs. Non-integrated signal at worst case φ with varying f_i ($A_{sig} = 1$ mV, $A_{intf} = 10$ mV).

AM is used for broadcasting in the medium wave range from 0.5 MHz to 1.7 MHz and shortwave range from 5.9 MHz to 26.1 MHz. Since shortwave range is closer to the antenna frequency of human body of around 40 MHz, for our analysis of I-DDR receiver in presence of AM interference, we use a carrier frequency$(f_i) = 20$ MHz. The reasonable modulation frequency (f_m) for such a carrier frequency is less than 5 kHz, so we choose $f_m = 2.5$ kHz as an example of a practical scenario. But for better illustration of robustness of I-DDR receiver to AM interference, we also provide simulation results in a scenario with$f_m = 2$ MHz.

Figure 5a shows the dependence of integrated interference (IS_{intf}) on the ratio of integration period and interference period $(\frac{t}{T_i})$. For any arbitrary carrier phase (φ) or modulating signal phase (φ_m), the integrated interference does not exactly go to 0 for an integration period, which is an integral multiple of the interference period $(T_b = nT_i)$. Figure 5b shows the relative interference rejection of the I-DDR receiver with frequency in presence of an AM interference with carrier frequency of 20 MHz and modulation frequency of 2 MHz. Although the maximum rejection notch locations are not exactly at integral multiples of the interference carrier frequency, the relative rejection is >10 dB even for frequencies $\pm 10\%$ away from the interference carrier frequency. Also there is one notch corresponding to each integral multiple of the interference carrier frequency. Figure 5c analyzes the relationship of modulation frequency and relative interference rejection for different bit period for a given interference, since it may not be always possible to have an accurate sampling at $T_b = nT_i$. A smaller modulation frequency results in smaller residual integrated interference at the sampling instant. Hence, the I-DDR receiver provides better interference rejection in those scenarios. For a practical scenario in the shortwave range, where $f_m = 2.5$ kHz and $f_i = 20$ MHz, the rejection is greater than 17dB even for a frequency $\pm 10\%$ away from the notch frequency (Figure 8a). Figure 5d shows a comparison of SIR at the sampling instant for non-integrated and integrated signal as the interference frequency is varied. It can be seen that even for the worst case phase, the integrated signal still ensures at least 24 dB improvement in integrated SIR for sampling at $T_b = T_i$. However, the relative interference rejection at the sampling instant $T_b = T_i$ is strongly dependent on the phase of the carrier and modulating wave as can be seen from Figure 6a. In the special scenario of a modulation phase, $\varphi_m = \pi$ the relative interference rejection is high, independent of the carrier

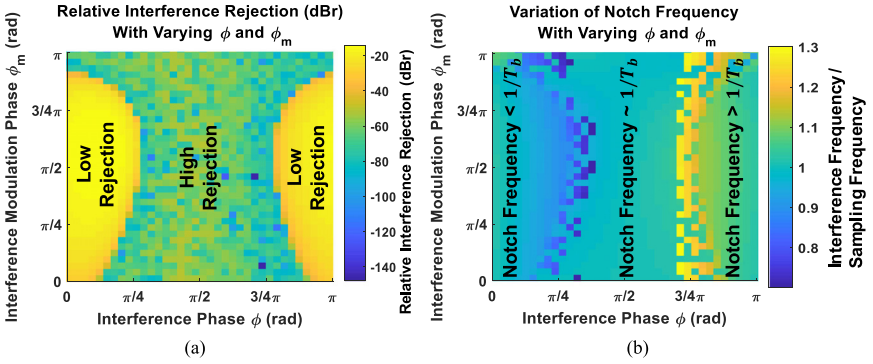

Fig. 6. Transfer function notch under AM interference with varying φ and φ_m ($f_m = 2$ MHz). a) Transfer function notch value in dB b) Location of notch frequency with respect to data frequency of $1/T_b$.

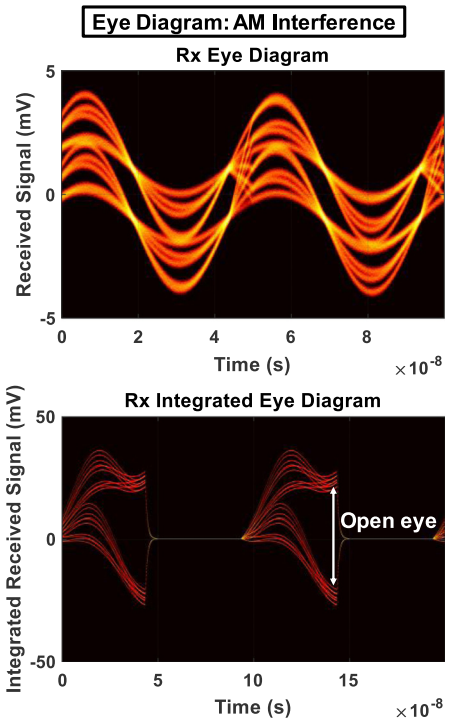

Fig. 7. Eye diagram comparison with and without integration ($A_{sig} = 1$ mV, $A_{intf} = 3$ mV, $K_{intf} = 10$) a) Non-integrated eye diagram in presence of AM interference b) Integrated eye diagram in presence of same interference.

phase (φ), which can be attributed to the low residual integrated interference under this condition as in (12). The variation of location of the transfer function notch frequency with modulation and carrier wave phase is shown in Figure 6b. The notch is located at the interference frequency for $\varphi = \frac{\pi}{2}$, independent to φ_m. The notch frequency is lower than the interference frequency for $< \frac{\pi}{2}$, whereas it becomes higher for $\varphi > \frac{\pi}{2}$. The non-integrated and integrated received eye diagrams are plotted in Figure 7a, b respectively. The integrated eye diagram shows clear eye opening enabling correct sampling whereas the non-integrated eye diagram is completely closed. This validates the interference rejection property of the I-DDR receiver in presence of AM interference and the potential SIR improvement achieved from it.

Analysis of I-DDR principle: FM interference

$$S_{intf}(t) = A_{intf}\cos(\omega_i t + B\sin(\omega_m t) + \varphi)$$

$$= A_{intf}\sum_{k=-\infty}^{\infty} J_k(B)\cos((\omega_i + k\omega_m)t + \varphi), \quad \forall t \quad (15)$$

$$\omega_i = \frac{2\pi}{T_i} = \text{Carrier Wave Frequency},$$

$$\omega_m = \frac{2\pi}{T_m} = \text{Modulation Wave Frequency},$$

$$B = \frac{A_m \Delta f}{f_m},\ \Delta f = \text{Frequency Deviation}$$

$$IS_{intf}(t) = \int_0^t S_{intf} \quad (16)$$

$$= \begin{cases} K_{int}A_{intf}\sum_{k=-\infty}^{\infty} J_k \\ (B)\frac{\sin((\omega_i + k\omega_m)t+\varphi)}{\omega_i + k\omega_m}, & 0 \le t \le T_b \\ 0, & T_b \le t \le 2T_b \end{cases}$$

$$IS_{intf}|_{t=T_b} = K_{int}A_{intf}\sum_{k=-\infty}^{\infty} J_k(B)$$

$$\frac{\sin((\omega_i + k\omega_m)T_b + \varphi) - \sin(\varphi)}{\omega_i + k\omega_m} \quad (1)$$

$$= K_{int}A_{intf}\sum_{k=-\infty}^{\infty} J_k(B)$$

$$\frac{\sin\left(2\pi k\frac{T_b}{T_m} + \varphi\right) - \sin(\varphi)}{\omega_i + k\omega_m},\ \forall T_b; \quad (2)$$

$$= nT_i;\ n = \text{positive integer} \quad (17)$$

SIR without integration

$$= \frac{\pm A_{sig}}{A_{intf}\sum_{k=-\infty}^{\infty} J_k(B)\cos((\omega_i + k\omega_m)t + \varphi)} \quad (18)$$

Integrated SIR $=$

$$\frac{\pm A_{sig}T_b}{A_{intf}\sum_{k=-\infty}^{\infty} J_k(B)\frac{\sin\left(2\pi k\frac{T_b}{T_m} + \varphi\right) - \sin(\varphi)}{\omega_i + k\omega_m}} \quad (19)$$

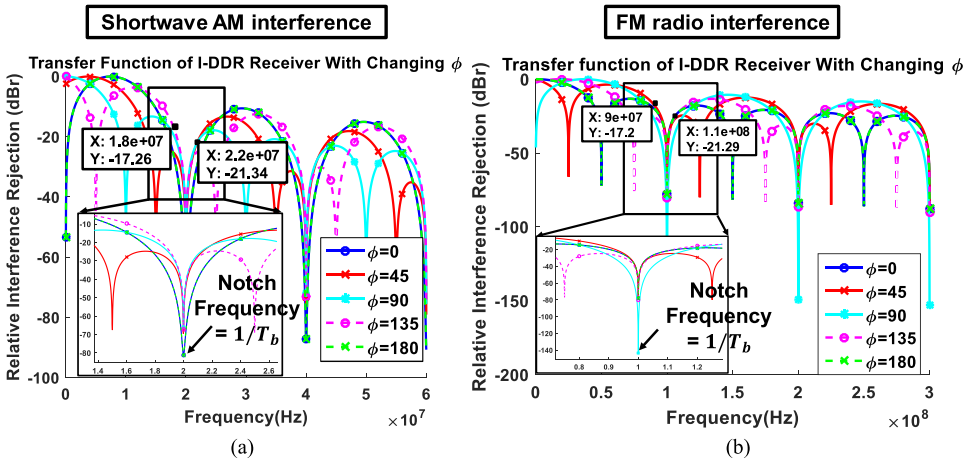

Fig. 8. I-DDR receiver transfer function under realistic scenario for AM and FM interference a) AM: $f_i = 20$ MHz, $f_m = 2.5$ kHz b) FM: $f_i = 100$ MHz, $f_m = 25$ kHz. The transfer function notch frequency stays at $1/T_b$, similar to continuous wave scenario.

Key Takeaway: The presence of AM interference, with high enough modulation frequency, moves the frequency notch away from the data frequency $(f = \frac{1}{T_b})$. The position of the notch is dependent on the interference carrier and modulation frequency but provides at least 20dB rejection at $f = \frac{1}{T_b}$ for all scenarios. For a realistic scenario with shortwave AM, the movement of the notch is minimal due to low modulation frequency.

D. Frequency Modulated (FM) Interference

The performance of I-DDR receiver in presence of FM interference is analyzed in this section. The FM interference is approximated using Bessel function (J_k) as in (15). For existing FM bands of 88–110 MHz, the channel bandwidth (BW) is 200 kHz and the maximum frequency deviation (Δf) is 75 kHz, which translates to a modulation index (B) of 3. However, we also simulate using an FM signal with high modulation frequency of $f_m = 10$ MHz for analyzing the interference robustness of the I-DDR receiver. The modulation index B is chosen as 0.5 in this scenario to compare the performance of I-DDR receiver in presence of AM and FM interference of same modulation index. The integrated interference and SIR with and without integration are as shown in (16)–(19). For all our simulations of FM interference, we choose to use the first 7 terms $(k = 0, \pm 1, \ldots, \pm 6)$ of the Bessel expansion.

Figure 9a shows that under FM interference also the integrated interference is nearly 0 for any φ if the bit period is chosen as $T_b = nT_i$. Figure 9b shows that the relative rejection of the integrated and sampled interference is always greater than 19 dB in the FM radio frequency band of 88–110 MHz even if the modulation frequency (f_m) is taken as 10 MHz. The relative interference rejection reduces as the FM modulation frequency increases as can be seen in Figure 9c. This also shows that, even with $\pm 10\%$ sampling error due to jitter and non-idealities, >11 dB interference suppression can be achieved for modulation frequencies up to 10 MHz. Figure 9d shows the SIR comparison between integrated and non-integrated receiver with sampling at $T_b = T_i$. There is a 22 dB improvement in SIR achievable through integration in presence of FM interference. In a practical scenario with small modulation frequency (25 KHz), there exists a notch in the I-DDR transfer function for frequencies which are an integral multiple of the interference frequency, independent of the phase of the interference signal (Figure 8b). For higher modulation frequency (10 MHz) on the other hand, the notch frequency with the highest rejection is dependent on the initial phase of the interference and can be $>10\%$ away from the interference carrier frequency (f_i) as can be seen in Figure 10b. Figure 10a shows the interference rejection of I-DDR receiver at the interference carrier frequency with varying carrier phase of the FM interference. It demonstartes that the carrier phase doesn't have much effect on the relative interference rejection and >60 dB interference rejection can be achieved at interference frequency for any relative phase difference between the data and interference. Similar to AM interference the integrated eye diagram shows clear eye opening in presence of FM interference (Figure 11b), whereas the non-integrated eye is almost completely closed (Figure 11a).

Key Takeaway: In presence of FM interference with high modulation frequency, the transfer function notch of the I-DDR receiver does move away from the data frequency $(f = \frac{1}{T_b})$. However there is at least one notch within $\pm 5\%$ of the data frequency (Figure 9b). This shift is considerably less than AM interference which can show up to $\pm 30\%$ shift in notch frequency (–Figure 5b, Figure 6b). Since AM results in varying amplitude of the interference and the residual of integration is affected more by amplitude of interference than its frequency variation (as in FM interference), the movement of notch away from the data frequency is more in case of AM interference.

IV. Discussion

A. Experimental Method

The I-DDR principle is validated using actual HBC signals transferred through the body. The HBC channel loss shows day to day and person to person variation. Hence, HBC channel loss measurement studies require multiple experiments to be run over

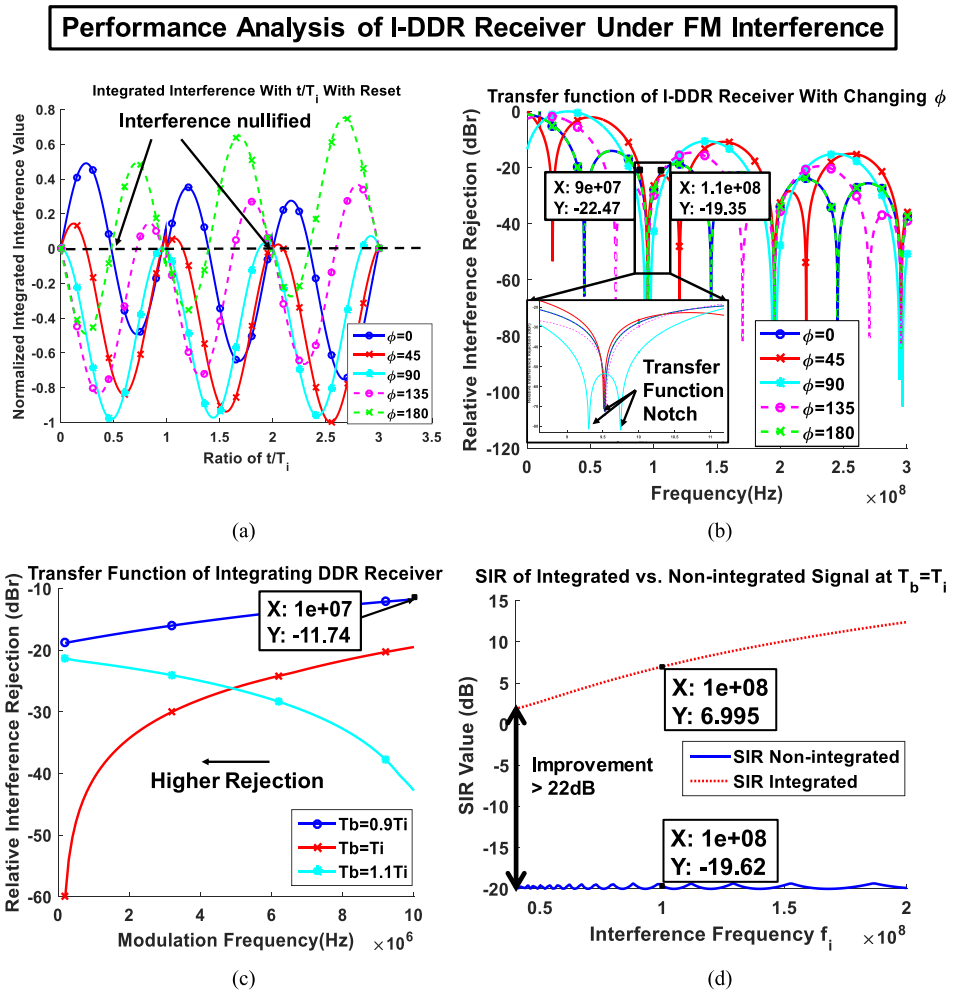

Fig. 9. Performance analysis of I-DDR receiver under FM interference ($f_i = 100$ MHz, $f_m = 10$ MHz, $B = 0.5$, $N = 7$) a) Integrated interference (IS_{intf}) as a function of $\frac{t}{T_i}$ with reset b) Interference suppression as a function of interferer frequency with changing φ c)Worst case Interference rejection as a function of modulation frequency in presence of $\pm 10\%$ sampling mismatch. d) Worst case SIR of Integrated vs. Non-integrated signal with varying f_i ($A_{sig} = 1$ mV, $A_{intf} = 10$ mV).

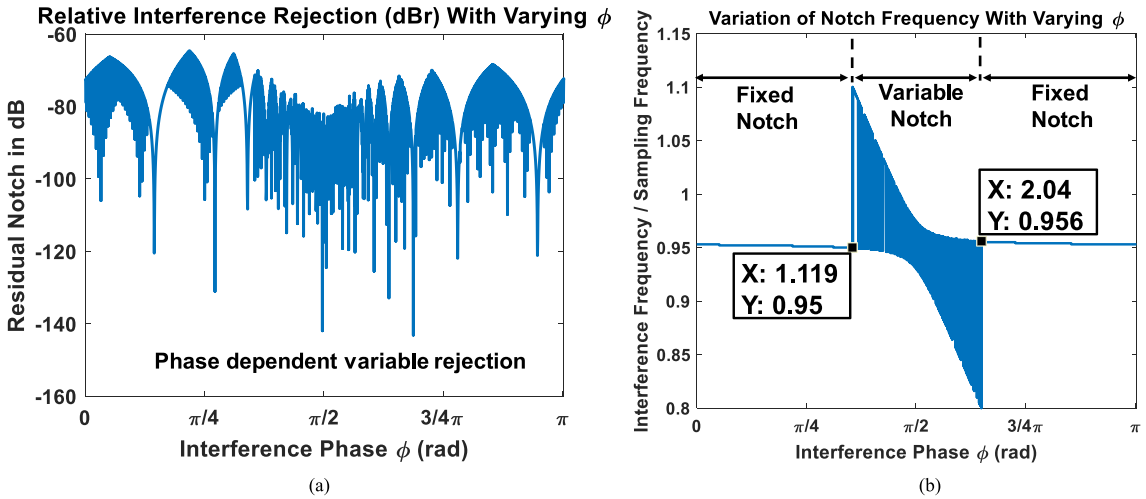

Fig. 10. Residual notch under FM interference with varying φ and φ_m ($f_i = 100$ MHz, $f_m = 10$ MHz, $B = 0.5, N = 7$) a) Residual value in dB b) location of maximum rejection notch as a ratio of interference frequency (f_i) and sampling frequency (f_b).

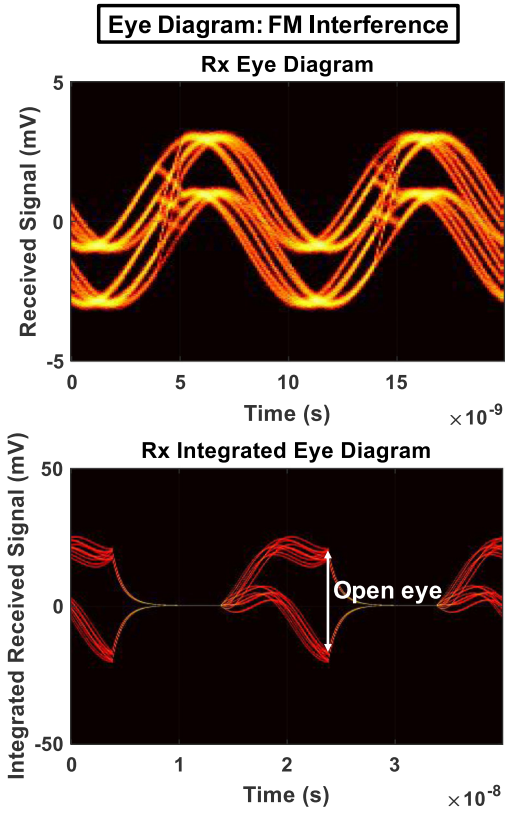

Fig. 11. Eye diagram comparison with and without integration ($A_{sig} = 1$ mV, $A_{intf} = 3$ mV, $K_{intf} = 10$) a) Non-integrated eye diagram in presence of FM interference b) Integrated eye diagram in presence of same interference.

multiple subjects on multiple days to measure the average and variation of channel loss and provide statistical significance to the results. However, for our experiments HBC signals are used only to capture the effect of channel loss on the transmitted signal and the day to day channel loss variation is not critical for the validity of the I-DDR principle. Hence, the experiments are not carried out on multiple subjects and are carried over three different measurements on the same person.

B. Clock-Data Phase Alignment: Clock Data Recovery

The output of the integration operation at the front-end is dependent on the phase relation between the integrator clock and data. Since the integration operation is an accumulation of the voltage level over time, any relative phase mismatch between integrator clock and data will directly reflect in the integrated voltage amplitude. The integrator output is maximized when the integration operation starts at the beginning of the data period and continues over the complete data period. This requires appropriate phase and frequency relation between the data and the integrating clock. This can be achieved through a Clock Data Recovery (CDR) loop commonly used in broadband wireline receivers [16]–[18]. In a traditional CDR loop, the sampling clock is aligned with the middle of the data period. However, in the current scenario of the integrating receiver, the sampling clock is aligned with the beginning of the data period. The CDR loop utilizes a phase frequency detector to find the phase mismatch between clock and data and convert it to a voltage, which is then utilized to control the frequency of a Voltage Controlled Oscillator (VCO). The VCO frequency is controlled to enable phase alignment between the clock and the data by moving the clock phase. Alternatively a phase interpolator can also be used to move the phase of the integrating clock to align with the beginning of the data period. A detailed analysis of clock data phase recovery through an Integrating Mueller-Muller CDR for the I-DDR receiver is presented in [19].

V. Measurements: Validation of I-DDR Principle

A. COTS Component based Measurements

Figure 12 shows the conceptual diagram of the measurement set up and is used to verify the interference robustness of the proposed *I-DDR* receiver. Data and interference are injected into the body through two separate electrodes. A TIVA-C 123GXL microcontroller board is used to apply a Pseudo Random Bit Sequence (PRBS) at a data rate of 1 Mbps. The PRBS bit sequence is coupled to the body through a copper electrode connected to a band. The electrodes are custom made and have a size of 2 cm $\times$ 2 cm. The transmitter transmits a voltage of 1V. This emulates the voltage transmission from a custom Integrated Circuit fabricated in TSMC 65 nm technology, which typically has a supply voltage around 1V. A battery operated signal generator is used to apply interferences of different amplitude and frequency. The interference is coupled to the body through a separate band containing an electrode. Although in an actual HBC scenario the interference will be picked up due to the human body antenna effect, we use a third electrode to inject an interference with known parameters. The response of the I-DDR receiver is independent of the coupling mechanism. Hence, introducing the interference through a third electrode in a controlled manner will help us to quantitatively characterize the interference rejection capability of the I-DDR principle. The received signal was captured in an oscilloscope through a similar band. To emulate the scenario of actual HBC between wearable devices, battery operated signal generator is used to apply interferences of different amplitude and frequency. The interference is coupled to the body through a separate band containing an electrode. The received signal is captured through an oscilloscope and integrated. Using a large power supply connected device to capture signals does not completely reflect an actual HBC scenario for communication between two wearable devices and can affect the HBC channel loss, as previously reported in [4], [8], [10], [20]. Previous studies [8], [10] report up to 9 dB reduction in channel loss due to the introduction of ground connected instruments in the measurement setup. To take care of the extra loss, the integrated signal fed from the oscilloscope was attenuated, while applying to MATLAB for processing. The attenuated signal is processed in MATLAB through periodic reset, according to the working principle of the *I-DDR* receiver. Subsequently the eye diagram is plotted and the eye height is measured, as a measure of the interference rejection property of the receiver. The I-DDR operation of integration with periodic reset is achieved through

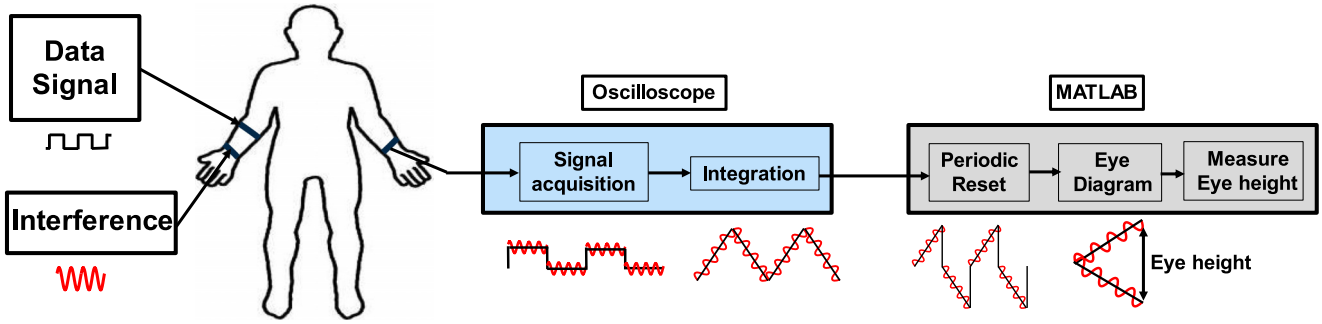

Fig. 12. Measurement setup diagram showing interference being injected along with the data signal and the combined signal being received at the oscilloscope. which is post processed according to the I-DDR principle to create the received eye diagram.

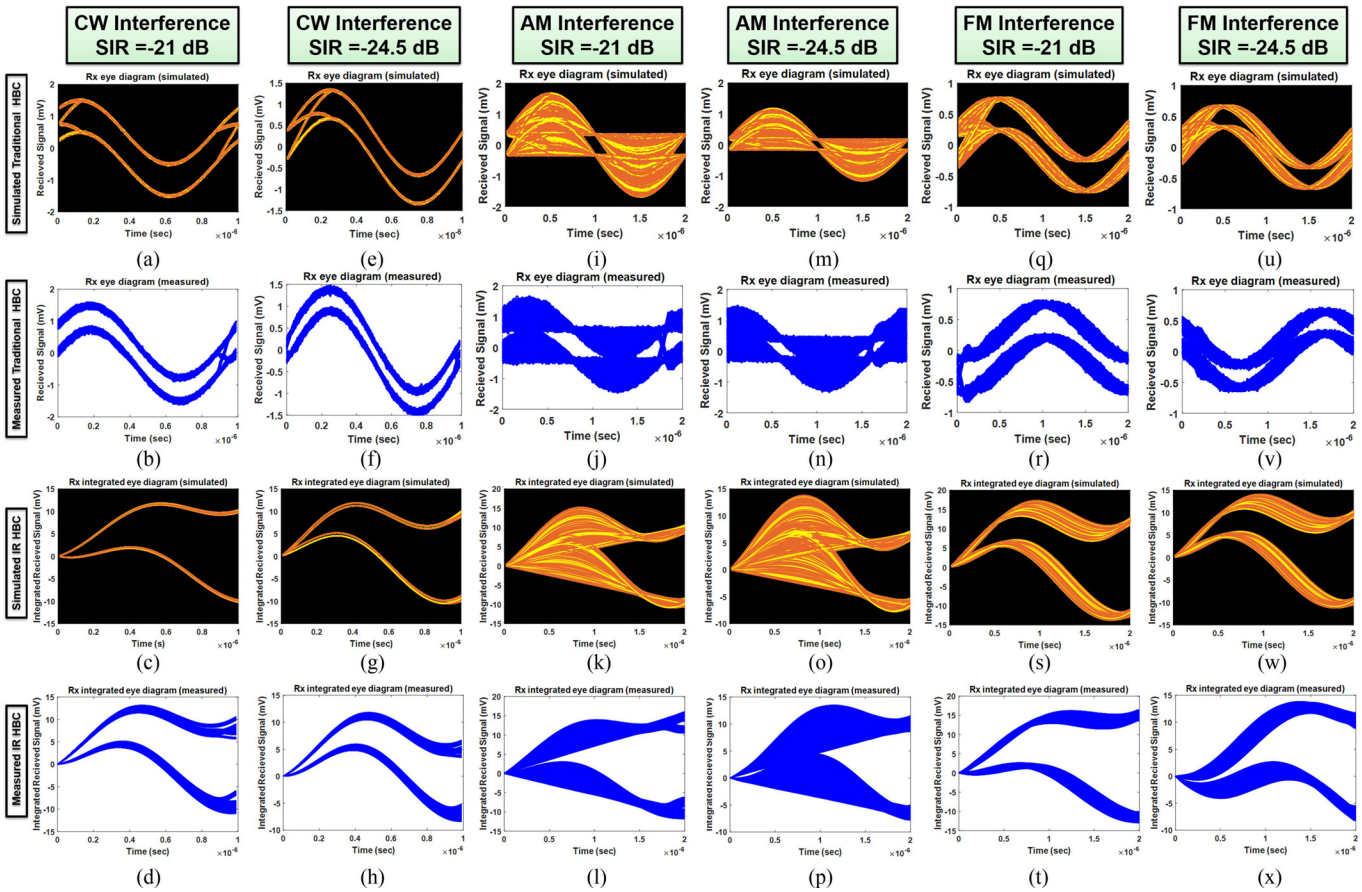

Fig. 13. Comparison results between simulated and measured eye diagram for HBC signaling under different interference conditions ($K_{intf} = 10$). NRZ signal + CW interference with SIR $= -21$dB a) Simulated Rx eye diagram b) Measured Rx eye diagram c) Simulated eye diagram of integrated Rx signal d) Measured eye diagram of integrated Rx signal. e)-h) Similar plots as a)-d) for NRZ signal + CW interference of SIR $= -24.5$dB. i)-l) Similar plots for NRZ signal + AM interference with SIR $= -21$dB, modulating carrier frequency of 18 KHz with modulation index 1. m)-p) Similar eye diagrams corresponding to NRZ signal + AM interference with SIR $= -24.5$dB. q)-t) Eye diagrams for NRZ signal + FM interference with SIR $= -21$ dB, modulating frequency 18KHz and frequency deviation 5 KHz. Integrated eye is significantly less affected compared to the NRZ eye. u)-x) Similar eye diagrams for NRZ signal + FM interference with SIR $= -24.5$dB. In all the different conditions the simulated and measured eye diagram shows close correspondence. The integrated eye shows higher opening than the normal eye under CW, AM, FM interference condition proving the efficacy of the *I-DDR* receiver principle.

integral function in the oscilloscope and achieving the periodic reset operation by processing the integrated signal from oscilloscope in MATLAB. Although this setup doesn't contain the circuit-level non-idealities of a hardware implementation of the integrator, it enables validating the applicability of the I-DDR principle on signals transmitted through the body.

Figure 13 shows the eye diagrams obtained from the measured signals while applying CW, AM and FM interference corresponding to two different SIR values. Due to the limitation of the signal generator we could not reach 100Mbps data rate or apply an interference signal of 100 MHz. But we have taken the data rate and interference in such a way that the symbol duration

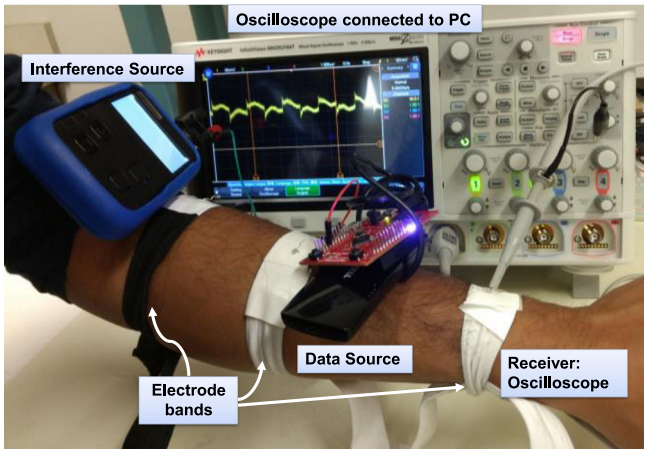

Fig. 14. Actual measurement setup picture. The microcontroller board and signal generator is used to provide signal and interference through two separate electrodes. The received signal is captured in an oscilloscope and processed according to the I-DDR principle using MATLAB.

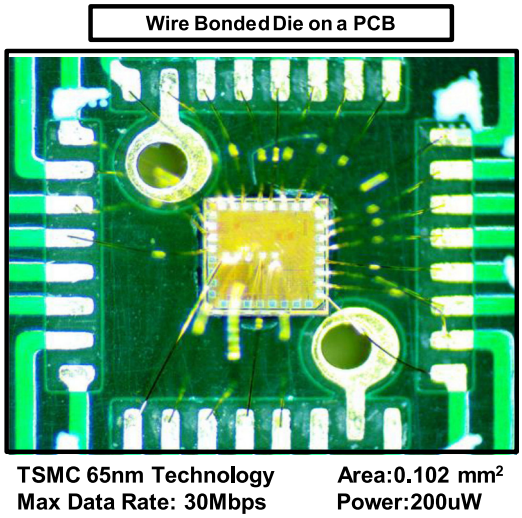

Fig. 15. Picture of the PCB containing the die with the I-DDR receiver fabricated in TSMC 65 nm technology. The die is wirebonded to the PCB.

remains an integral multiple of the interference time period and the theory of the *I-DDR* receiver can be validated. Figure 13a–13d correspond to the case when a CW interference of 1 MHz with SIR $= -21$ dB is applied to the body. Figure 13a shows the simulated eye diagram of the Rx NRZ signal, Figure 13b shows the eye diagram for the measured received signal under the same condition. Figure 13c, d shows the integrated eye diagram from simulation and from measurement. The eye height of the measured and simulated eye diagrams show that the integrated eye height is more than the normal Rx eye. Figure 13e–13h shows the simulated and measured eye diagrams for CW interference of SIR $= -24.5$ dB. In both cases the integrated eye shows larger opening than the Rx eye. Figure 13i–13p correspond to the measured and simulated Rx and integrated eye diagram for AM interference of two different SIR. The frequency of the carrier signal is 500 KHz and the modulating signal is a sine wave of 18 KHz with modulation index 1. Figure 13q–13x corresponds to the measured and simulated eye diagram for FM interference corresponding to two different SIR conditions. The frequency of the carrier signal is 500 KHz and the maximum frequency deviation is 5 KHz with a modulating carrier frequency of 18 KHz. In all the cases the measured and the simulated eye heights match closely. Also the eye height measurements show that even with injected interference the *I-DDR* receiver performs better than a normal receiver and the eye diagrams show significant eye opening. Figure 14 shows an actual picture of the setup used for measurements.

B. Integrated Circuit Based Measurements

This subsection looks into measurements of the interference rejection property of the I-DDR receiver through an integrated circuit. The measurement setup is similar to that shown in Figure 12, but in this case the operation of the oscilloscope and MATLAB in PC is replaced by an I-DDR receiver, fabricated in TSMC 65 nm technology (Figure 15). The detailed architecture and design of the receiver are explained in [11]. The goal

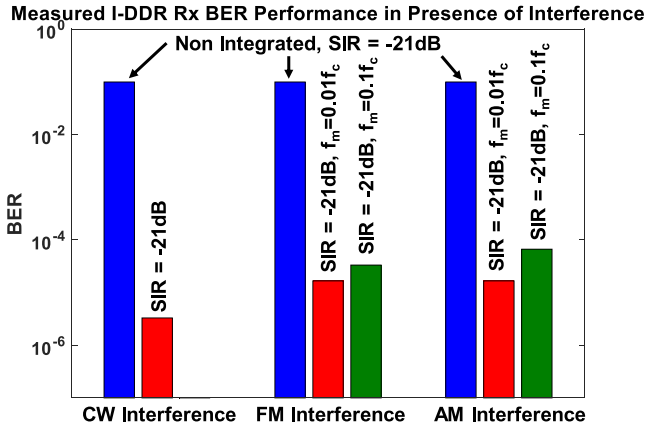

Fig. 16. Measured BER performance of an I-DDR receiver fabricated in TSMC 65 nm Technology. The carrier frequency of the different type of interferences is kept at 6 MHz, the modulation index $= 0.5$ (AM or FM) and the data rate fixed at 6Mbps. Scenarios with higher modulation frequency (for AM and FM) shows higher BER as the frequency rejection notch moves further away from the desired point corresponding to the data rate.

of this paper is to develop a theoretical understanding of I-DDR receiver's performance under varying AM, FM interference conditions like modulation frequency, modulation index etc. Hence, the Bit Error Rate (BER) performance of the receiver is evaluated as a measure of the interference rejection capability of the receiver. A PRBS data sequence is generated at the transmitter, which is then transmitted through the body after being injected with interference and decoded at the receiver. The received data sequence is compared with the expected bit sequence to measure the BER. A lower BER indicates higher interference rejection at the receiver end. Figure 16 shows the measured BER of the receiver under different interference scenarios. Without integration, the BER at the receiver is high ($\sim 10^{-1}$) in presence of any kind of interference. Under Continuous Wave interference with SIR $= -21$dB, the integrating receiver shows substantial

improvement in BER performance ($<10^{-5}$), demonstrating interference rejection. Similar performance enhancement can be seen in presence of AM and FM interference. Experiments are carried out with FM interference of 6 MHzcarrier frequency and two different modulation frequencies: 600 KHz and 60 KHz. The data rate is kept fixed at 6 Mbps such that there is an interference rejection notch around the carrier frequency of 6 MHz. It can be seen that the BER is less for lower modulation frequency as the frequency notch is closer to the carrier frequency. Similarly for FM interference, the BER is lower in case of a lower modulation frequency as expected from the theoretical analysis. However, it is interesting to note that the BER is higher in presence of AM interference compared to FM interference. As previously discussed in subSection III.D, simulation results show that the frequency notch moves further away from the carrier frequency in presence of AM interference compared to FM. Hence the frequency rejection at the carrier frequency will be lower in presence of AM interference compared to FM interference.

VI. Conclusion

Human Body Communication has emerged as a strong contender for connecting wearable devices and sensors due to its low-power, security properties. The antenna property of human body, which makes it pickup ambient interference, has limited HBC implementation to mostly narrowband techniques. The I-DDR receiver provides a broadband interference robust implementation, which can enable improved energy efficient HBC systems. We analyzed the performance of the I-DDR receiver, through theoretical derivation and system analysis in presence of CW, AM and FM interference and show >22 dB improvement in interference tolerance. Experiments were carried out by transmitting HBC data along with injected interference. Measurements from both COTS and IC based implementations show the efficacy of the I-DDR principle in rejecting CW, AM and FM interference even under conditions with SIR of -21 dB. This paper provides a detailed theoretical analysis of the I-DDR receiver, validated through simulations and experiments. While the effect of circuit level non-idealities like timing mismatch can be explained through this analysis, other effects like nonlinearity, saturation of circuits is not completely captured and is outside the scope of this paper.

References

[1] S. Sen, "SocialHBC: Social networking and secure authentication using interference-robust human body communication," in *Proc. Int. Symp. Low Power Electron. Design*, 2016, pp. 34–39.

[2] N. Cho, L. Yan, J. Bae, and H. J. Yoo, "A 60 kb/s-10 Mb/s adaptive frequency hopping transceiver for interference-resilient body channel communication," *IEEE J. Solid-State Circuits*, vol. 44, no. 3, pp. 708–717, Mar. 2009.

[3] H. Cho, H. Kim, M. Kim, J. Jang, J. Bae, and H. J. Yoo, "21.1 A 79 pJ/b 80Mb/s full-duplex transceiver and a 42.5 uW 100kb/s super-regenerative transceiver for body channel communication," in *Proc. IEEE Int. Solid-State Circuits Conf.*, 2015, pp. 1–3.

[4] Ž. Lucev, I. Krois, and M. Cifrek, "A capacitive intrabody communication channel from 100 kHz to 100 MHz," *IEEE Trans. Instrum. Meas.*, vol. 61, no. 12, pp. 3280–3289, Dec. 2012.

[5] J. Bae, H. Cho, K. Song, H. Lee, and H. Yoo, "The signal transmission mechanism on the surface of human body for body channel communication," *IEEE Trans. Microw. Theory Tech.*, vol. 60, no. 3, pp. 582–593, Mar. 2012.

[6] J. Hwang, T. Kang, Y. Kim, and S. Park, "Measurement of transmission properties of HBC channel and its impulse response model," *IEEE Trans. Instrum. Meas.*, vol. 65, no. 1, pp. 177–188, Jan. 2016.

[7] N. Cho, J. Yoo, S. Song, J. Lee, S. Jeon, and H. Yoo, "The human body characteristics as a signal transmission medium for intrabody communication," *IEEE Trans. Microw. Theory Tech.*, vol. 55, no. 5, pp. 1080–1086, May 2007.

[8] J. Park, H. Garudadri, and P. P. Mercier, "Channel modeling of miniaturized battery-powered capacitive human body communication systems," *IEEE Trans. Biomed. Eng.*, vol. 64, no. 2, pp. 452–462, Feb. 2017.

[9] Y. Song, Q. Hao, and K. Zhang, "Review of the modeling, simulation and implement of intra-body communication," *Defence Technol.*, vol. 9, no. 1, pp. 10–17, Mar. 2013.

[10] S. Maity *et al.*, "BioPhysical modeling, characterization and optimization of electroquasistatic human body communication," *IEEE Trans. Biomed. Eng.*, p. 1, 2018.

[11] S. Maity, B. Chatterjee, G. Chang, and S. Sen, "A 6.3 pJ/b 30 Mbps -30 dB SIR-tolerant broadband interference-robust human body communication transceiver using time domain signal-interference separation," in *Proc. IEEE Custom Integr. Circuits Conf.*, 2018, pp. 1–4.

[12] S. Maity, D. Das, and S. Sen, "Wearable health monitoring using capacitive voltage-mode human body communication," in *Proc. IEEE 39th Annu. Int. Conf. Eng. Med. Biol. Soc.*, 2017, pp. 1–4.

[13] J. Bae, K. Song, H. Lee, H. Cho, and H. J. Yoo, "A 0.24-nJ/b wireless body-area-network transceiver with scalable double-FSK modulation," *IEEE J. Solid-State Circuits*, vol. 47, no. 1, pp. 310–322, Jan. 2012.

[14] W. Saadeh, M. A. B. Altaf, H. Alsuradi, and J. Yoo, "A 1.1-mW ground effect-resilient body-coupled communication transceiver with pseudo OFDM for head and body area network," *IEEE J. Solid-State Circuits*, vol. 52, no. 10, pp. 2690–2702, Oct. 2017.

[15] J. Lee et al., "30.7 A 60 Mb/s wideband BCC transceiver with 150 pJ/b RX and 31 pJ/b TX for emerging wearable applications," in *Proc. IEEE Int. Solid-State Circuits Conf. Digest Tech. Papers*, 2014, pp. 498–499.

[16] C. Thakkar, S. Sen, J. E. Jaussi, and B. Casper, "23.2 A 32 Gb/s bidirectional 4-channel 4pJ/b capacitively coupled link in 14 nm CMOS for proximity communication," in *Proc. IEEE Int. Solid-State Circuits Conf.*, 2016, pp. 400–401.

[17] D. Kim, W. Choi, A. Elkholy, J. Kenney, and P. K. Hanumolu, "A 15 Gb/s 1.9pJ/bit sub-baud-rate digital CDR," in *Proc. IEEE Custom Integr. Circuits Conf.*, 2018, pp. 1–4.

[18] T. Musah *et al.*, "A 4-32 Gb/s bidirectional link with 3-tap FFE/6-tap DFE and collaborative CDR in 22 nm CMOS," *IEEE J. Solid-State Circuits*, vol. 49, no. 12, pp. 3079–3090, Dec. 2014.

[19] S. Maity, P. Mehrotra, and S. Sen, "An improved update rate baud rate CDR for integrating human body communication receiver," in *Proc. IEEE Biomed. Circuits Syst. Conf.*, 2018, pp. 1–4.

[20] M. A. Callejón, J. Reina-Tosina, D. Naranjo-Hernández, and L. M. Roa, "Measurement issues in galvanic intrabody communication: Influence of experimental setup," *IEEE Trans. Biomed. Eng.*, vol. 62, no. 11, pp. 2724–2732, Nov. 2015.

Shovan Maity (S'18) received the B.E. degree in electronics and telecommunication engineering from Jadavpur University, Kolkata, India, in 2012, and the M.tech. degree in electrical engineering from Indian Institute of Technology (IIT) Bombay , Mumbai, India, in 2014. He is currently working toward the Ph.D. degree in electrical engineering with Purdue University, West Lafayette, IN, USA. From 2014 to 2016, he was an Analog Design Engineer with Intel, Bangalore, India. His research interests include design of circuits and systems for human body communication, hardware security, and mixed signal circuits design. He is the recipient of the Institute Silver Medal, IIT Bombay in 2014 and the HOST 2017 best student paper award.

Xinyi Jiang (S'18) received the undergraduate degree in electrical engineering from Purdue University, West Lafayette, IN, USA, in 2017. She is currently working toward the master's degree with the University of California, Berkeley, Berkeley, CA, USA. She joined SPARC Lab, Purdue in spring 2016 and worked on Interference-Robust Human Body Communication. Her research interest is in Analog and Mixed-signal Circuit Design.

Shreyas Sen (S'06–M'11–SM'17) received the Ph.D. degree in electrical and computer engineering from Georgia Tech, Atlanta, GA USA, in 2011. He is currently an Assistant Professor with the School of Electrical and Computer Engineering, Purdue University, West Lafayette, IN, USA. He has more than five years of industry research experience with Intel Labs, Qualcomm and Rambus. He has authored/coauthored 2 book chapters, more than 100 conferences and journal papers, and has 13 patents granted/ pending. His research interests include mixed-signal circuits/systems for Internet of Things, biomedical and security. In 2018, He was chosen by MIT Technology Review as one of the top 10 Indian Inventors Worldwide under 35 (MIT TR35 India Award), for the invention of using the Human Body as a Wire, which has the potential to transform healthcare, neuroscience and human–computer interaction. He is a recipient of the AFOSR Young Investigator Award 2017, NSF CISE CRII Award 2017, Google Faculty Research Award 2017, Intel Labs Divisional Recognition Award 2014 for industry-wide impact on USB-C type, Intel PhD Fellowship 2010, IEEE Microwave Fellowship 2008, GSRC Margarida Jacome Best Research Award 2007, Best Paper Awards at HOST 2017 and 2018, ICCAD Best-in-Track Award 2014, VTS Honorable Mention Award 2014, RWS Best Paper Award 2008, Intel Labs Quality Award 2012, SRC Inventor Recognition Award 2008 and Young Engineering Fellowship 2005. He was as an Associate Editor for the IEEE Design & Test, Executive Committee member of the IEEE Central Indiana Section, ETS and Technical Program Committee member of DAC, CICC, DATE, ISLPED, ICCAD, ITC, VLSI Design, IMSTW, and VDAT.